Asian Journal of Chemistry; Vol. 32, No. 10 (2020), 2453-2459

ASIAN JOURNAL OF CHEMISTRY

https://doi.org/10.14233/ajchem.2020.22721

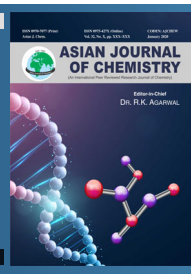

Glittering ZnO/Ag/MnO Nano Superstructures for Photocatalytic Applications

J.P. SHUBHA[1,*], S. SHWETHA PRIYADHARSHINI[2] and S. JAYADEV[2]

[1]Department of Chemistry, Don Bosco Institute of Technology (Affiliated to Visvesvaraya Technological University, Belagavi), Kumbalagodu, Mysore Road, Bangalore-560074 , India
[2]Department of Chemistry, S.J.B. Institute of Technology (Affiliated to Visvesvaraya Technological University, Belagavi), Kengeri, Bangalore-560060, India

*Corresponding author: E-mail: shubhapranesh@gmail.com

Received: 14 March 2020; *Accepted*: 14 May 2020; *Published online*: 25 September 2020; AJC-20052

ZnO/Ag/MnO ternary heterostructure nanomaterials have been synthesized *via* cost effective green route using zinc nitrate, manganese acetate and silver nitrate as oxidizers and perished curd as a fuel. The obtained ZnO/Ag/MnO nanomaterials are analyzed using Powder X-ray diffraction (PXRD), Fourier transform infrared spectroscopy (FTIR), morphological studies by scanning electron microscopy (FESEM), internal structure by transmission electron microscopy (TEM). Both PXRD and FESEM techniques were used to confirm the formation of particles and flakes composition of ZnO/Ag/MnO nanomaterials. Photocatalytic activity of ZnO/Ag/MnO was assessed by varying light source, hydrogen ion concentration, amount of catalyst and amount of dye. The ZnO/Ag/MnO nanoparticles exhibited an enhanced photodegradation of methylene blue dye under visible light.

Keywords: Ternary heterostructres, Hydrothermal method, Photocatalysis, Methylene blue, Visible light.

INTRODUCTION

The weaving mills are usually found in small towns either in cottages or houses of the owners. India has huge market for cotton stoles and these stoles are generally white in colour and later dyed to get desired colour. There are atleast two dyeing units for every 8-10 weaving units and the people working in these dyeing units are unaware of hazards of using synthetic dyes. The conventional methods of dyeing used, reduces the efficiency of dye solution and the remaining dye solution is discharged into drainages like domestic sewage without any effluent treatment. The negligent way of disposing effluents in dyeing industries are damaging the aquatic life. The main reason for improper disposal of waste is that the owners of dyeing industries cannot afford for effluent treatment.

The expenses incurred for treatment of dye effluent is very high, leading to major water pollution [1,2]. Simple oxidation methods were used to reduce toxicity caused by harmful dyes, which are discharged from dyeing units. But these methods are inadequate [3,4]. ZnO was used enormously to reduce water pollution due to its advantageous semiconducting properties [5-8]. Later attentions are shifted to other metal oxides *e.g.*, CeO_2 [9], TiO_2 [10,11] too. Among all the metal oxides, ZnO perfor-med well under UV light. To enhance the catalytic property of ZnO, several researchers [12-23] used doped forms of ZnO as photocatalysts. To enhance the efficiency of photo-catalyst two metal oxides are combined as composite and used as photocatalyst [24-33]. Furthermore, composite metal oxides, metallic particles are also introduced [34-37]. Since Sunlight has some amount of UV light, metal oxides are chosen in such a way that one metal oxide is UV active and the other one is visible active. In these new heterostructures, it is proved that there is a more possibility of separation of charge carriers by preventing recombination [36-38]. In present work, ZnO and MnO and silver particles were introduced to the ZnO/MnO composite system. In this case ZnO is UV active, while MnO is visible light active and silver particles were spread over the system. This system is more advantageous because maximum sunlight can be utilized by both metal oxides to degrade methy-lene blue dye.

EXPERIMENTAL

Zinc nitrate hexahydrate (Sigma-Aldrich: 98%), manganese acetate (Sigma -Aldrich: 98%) and silver nitrate (Sigma-Aldrich: 99%) were used as precursor materials. Synthetic wastewater sample was made by dissolving known quantity of methylene blue (SDFCL, India) in distilled water. Hydrogen ion concentration was maintained by using buffer tablets (pH 4 and pH 10, Loba Chemie). Whole studies were carried out with double distilled water.

Photocatalytic performance measurements: Plenty of sunlight is available in India during the months of April and May. Since intensity of the sunlight is more from 11.00 am to 2.00 pm, experiments were carried out during same time. Spherical shaped glass bowl of 250 mL capacity with flat bottom, magnetic stirrer (Make: Remi), magnetic bit and electric connection were used to conduct the experiments. Magnetic stirrer was used at 450 rpm. Methylene blue solution (5, 10, 15 and 20 ppm) at 20, 30, 40 and 50 mg of ZnO/Ag/MnO were used experiments. These solutions are aerated by keeping in the dark for 40 min. Then solutions are kept used for sunlight by constant stirring, at intervals of 30 min nearly 3 mL of aqueous mixture was collected form reaction solution and subjected to centrifugation. The clear solution was withdrawn and transferred to cuvette and absorption was measured with UV-visible spectrophotometer (Labman: LMSP-UV1900). The degradation (%) of the dye was determined using the following eqn.:

$$\text{Degradation (\%)} = \frac{C_i - C_f}{C_i} \times 100$$

where initial (C_i) and final (C_f) are the dye concentrations.

The studies were carried out by varying concentration of dye, catalyst, pH (2, 4, 7, 8 and 10) and light source on the degradation of methylene blue.

Instruments: Powder X-ray diffraction (PXRD) data were collected with a Bruker diffractometer (Cu$K\alpha$ (λ = 1.5406 Å) X-ray source). Fourier-transform infrared (FTIR) spectra were recorded with Bruker IFS 66 spectrometer. Scanning electron microscope (SEM) images were obtained with ZEISS Gemini SEM 500 microscope. Optical transmission spectra were recorded on a PerkinElmer UV-Vis spectrometer. Transmission electron microscope (TEM) images were recorded with a JEOL JEM-2100 PLUS, operating at 200 kV accelerating voltage.

Catalyst powder preparation: Silver doped ZnO/MnO nanoparticles were synthesized by hydrothermal method. In a typical process, the stoichiometric amounts of zinc nitrate, manganese acetate and silver nitrate were thoroughly dissolved in 8 mL of perished curd and 8 mL distilled water under constant stirring for about 20 min. The resulting solution mixture was shifted to a 20 mL Teflon-lined hydrothermal bomb and heated for 24 h at 130 ºC in a hot air oven. After completion of the reaction, hydrothermal bomb allowed to cool down. Obtained brown powder was thoroughly washed with water followed by ethanol and dried for overnight at 150 ºC. The resultant compound was used for detailed studies.

RESULTS AND DISCUSSION

XRD analysis: Fig. 1 shows the XRD patterns of ZnO, MnO and ZnO/Ag/MnO nanoparticles. The diffraction peaks in Fig. 1a indicated that the synthesized composite material is crystallized in the mixed form of hexagonal, orthorhombic and cubic structures of ZnO, MnO and Ag. Fig. 1b is the reference XRD pattern of ZnO obtained from ICSD which is hexagonal with the JCPDS card no. 5-664 and lattice parameters a = 3.249 Å and c = 5.205 Å, while the space group is $P6_3mc$. Similarly, Fig. 1c-d shows the powder diffraction pattern of MnO and Ag, which are in orthorhombic and cubic structures with JCPDS no: 4-326 and 4-783 taken as a reference.

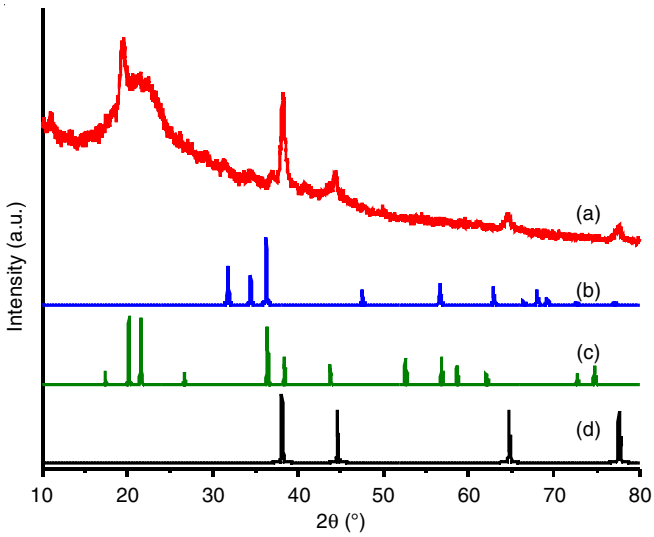

Fig. 1. XRD patterns of (a) ZnO/Ag/MnO nanoparticles, (b,c & d)ZnO, MnO and Ag-reference

FTIR analysis: FTIR spectrum of ZnO/Ag/MnO nanoparticles is recorded in the range 4000-400 cm^{-1} (Fig. 2). The characteristic peaks at 3793 and 1638 cm^{-1} are due to O-H stretching and H-O-H bending modes of vibrations, respectively. The peaks at ~2915 and 2847 cm^{-1} are attributed to C-H stretching modes of vibrations. A peak at ~2170 cm^{-1} may be due to C=O stretching of acetate. A peak around 1950 cm^{-1} can be assigned to C-H bending and a peak 1535 cm^{-1} may be attributed to N-O stretching of nitrate. The characteristic peaks at 741 and 723

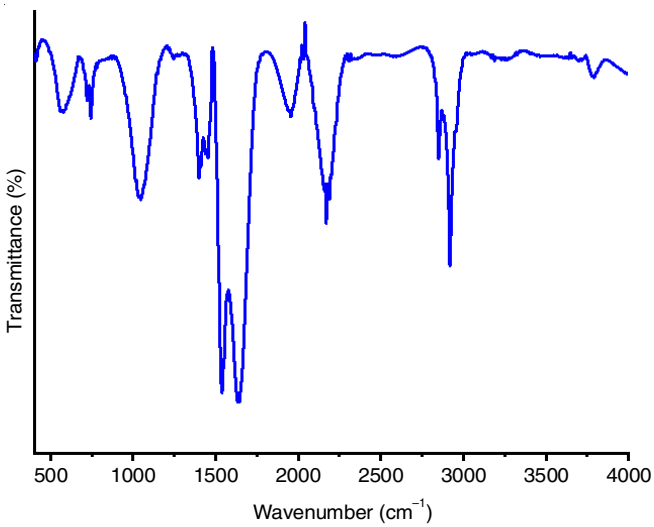

Fig. 2. FTIR spectrum of ZnO/Ag/MnO nanoparticles

cm^{-1} are due to Mn-O and Mn-O-Mn stretching modes of vibrational frequencies. A peak at 575 cm^{-1} is due to Zn-O stretching vibrations.

UV analysis: Fig. 3 shows the UV-visible absorption spectrum of as-prepared ZnO/Ag/MnO. The material shows the absorption range from 800 to 250 nm with maximum absorption at 420 nm, which shows that the material is more compatible to absorb wide range of light both from UV and Visible regions. Using Kulbeka-Munk equation, the band gap of the material was found to be 1.6 eV. A wide range of absorption of light helps in effective photocatalytic degradation and enhances the efficiency.

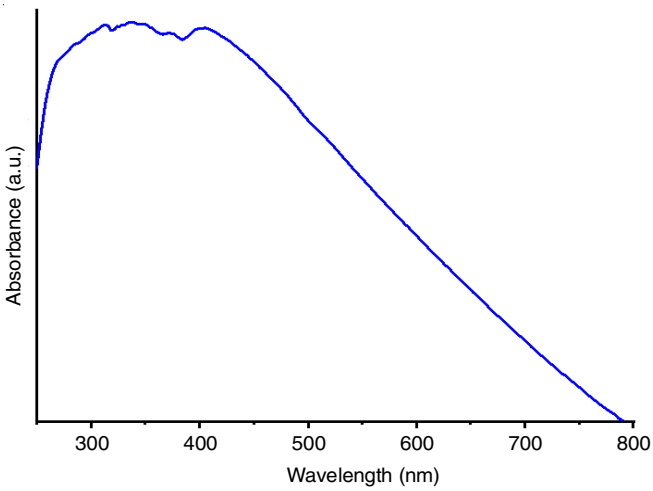

Fig. 3. UV-visible spectrum of ZnO/Ag/MnO nanoparticles

Morphological studies: The FESEM images of ZnO/Ag/MnO have been depicted in Fig. 4. A low magnified FESEM image of ZnO/Ag/MnO is shown in Fig. 4a, which shows the materials is composed in the form of particles as well as flakes. Fig. 4b is the high magnification FESEM image, which shows the part of the material is in the form of flakes in which all the flakes are interconnected and formed net like structure with large pores. Fig. 4c shows the high magnification image with spherical particles. We can anticipated that the ZnO and Ag formed as particles and MnO is evolved as flakes.

Fig. 5 shows the EDX spectrum of ZnO/Ag/MnO which designates that all the expected elements such as Zn, Mn, Ag, and O are present but couple of peaks is not designated with any symbols, which might be due to the presence silica as used as a substrate for the sample preparation. Elemental mappings of bulk ZnO/Ag/MnO have been collected and displayed in Fig. 6. It shows that the elements such as Zn, Mn, Ag and O are equally distributed all over the sample, which are indicated in different colours.

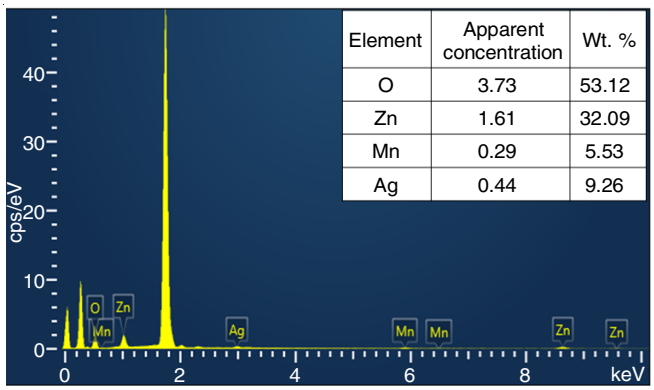

Element	Apparent concentration	Wt. %
O	3.73	53.12
Zn	1.61	32.09
Mn	0.29	5.53
Ag	0.44	9.26

Fig. 5. ED spectrum of ZnO/Ag/MnO nanoparticles with elements and their composition (inset table)

Fig. 7 shows the TEM images of ZnO/Ag/MnO nanoparticles. Fig. 7a-b showed the low and high magnification images, which demonstrated that the spherical particles are distributed all over the sample as well as sandwiched between the large sheets. The sizes of the particles are in the range between 20-60 nm and the sheets are in the range of few micrometers. The HRTEM image of ZnO/Ag/MnO (Fig. 7c) indicates that lattice fringes width is about 0.24 nm, signifies the presence of silver nanopar-ticles and belongs to (111) reflection plane of Ag. In addition, the selected area electron diffraction (SAED) pattern of the same compound is shown in Fig. 7d, which depicts that the material contains Ag existed in polycrystalline nature and the reflection planes were corresponded with XRD patterns.

Effect of light source: Under identical experimental conditions by keeping constant concentration of catalyst and dye

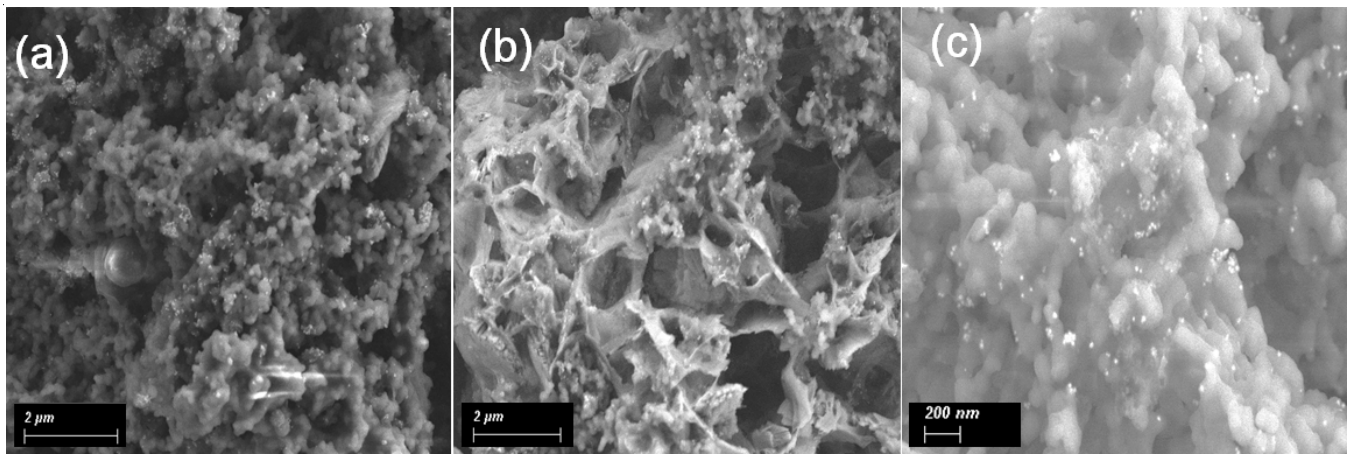

Fig. 4. FESEM images of ZnO/Ag/MnO nanoparticles with (a) low magnification, (b) high magnification showing flakes, (c) high magnification showing particles

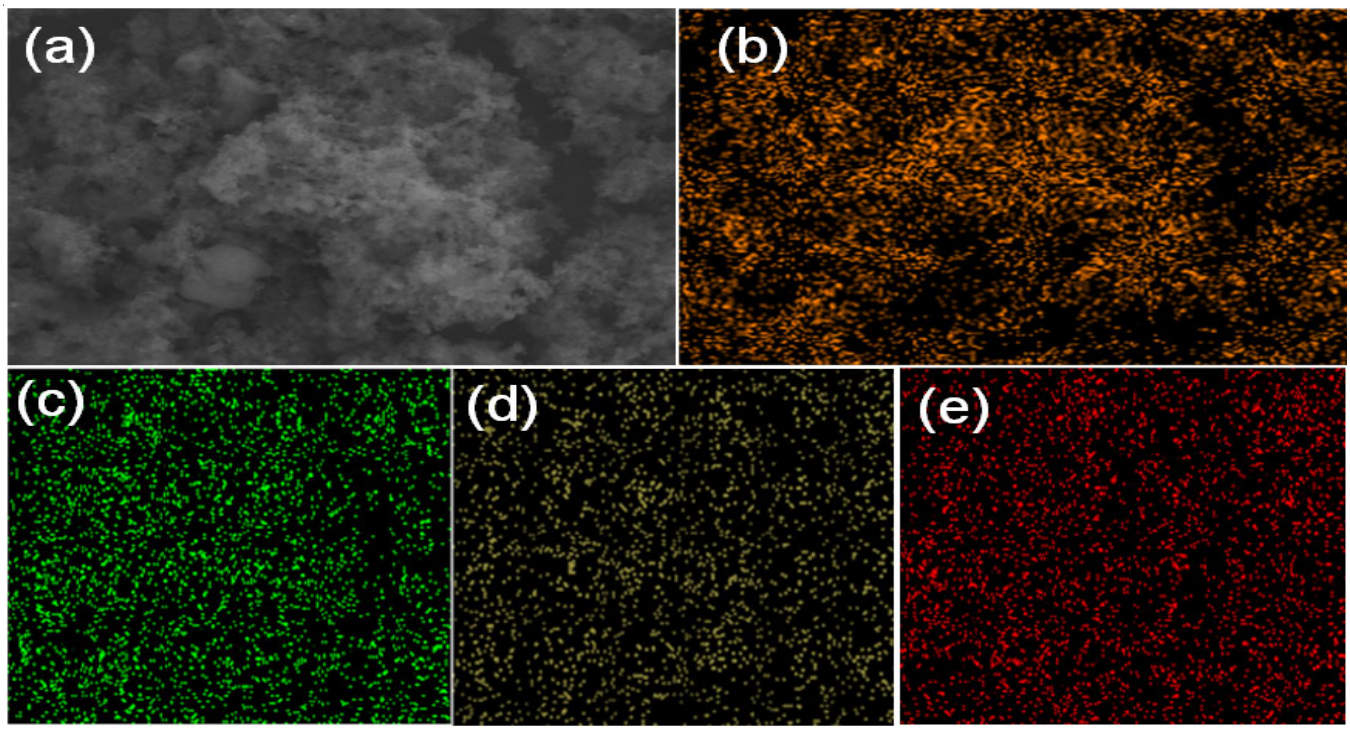

Fig. 6. Elemental mappings of (a) bulk, (b) O, (c) Zn, (d) Mn and (e) Ag

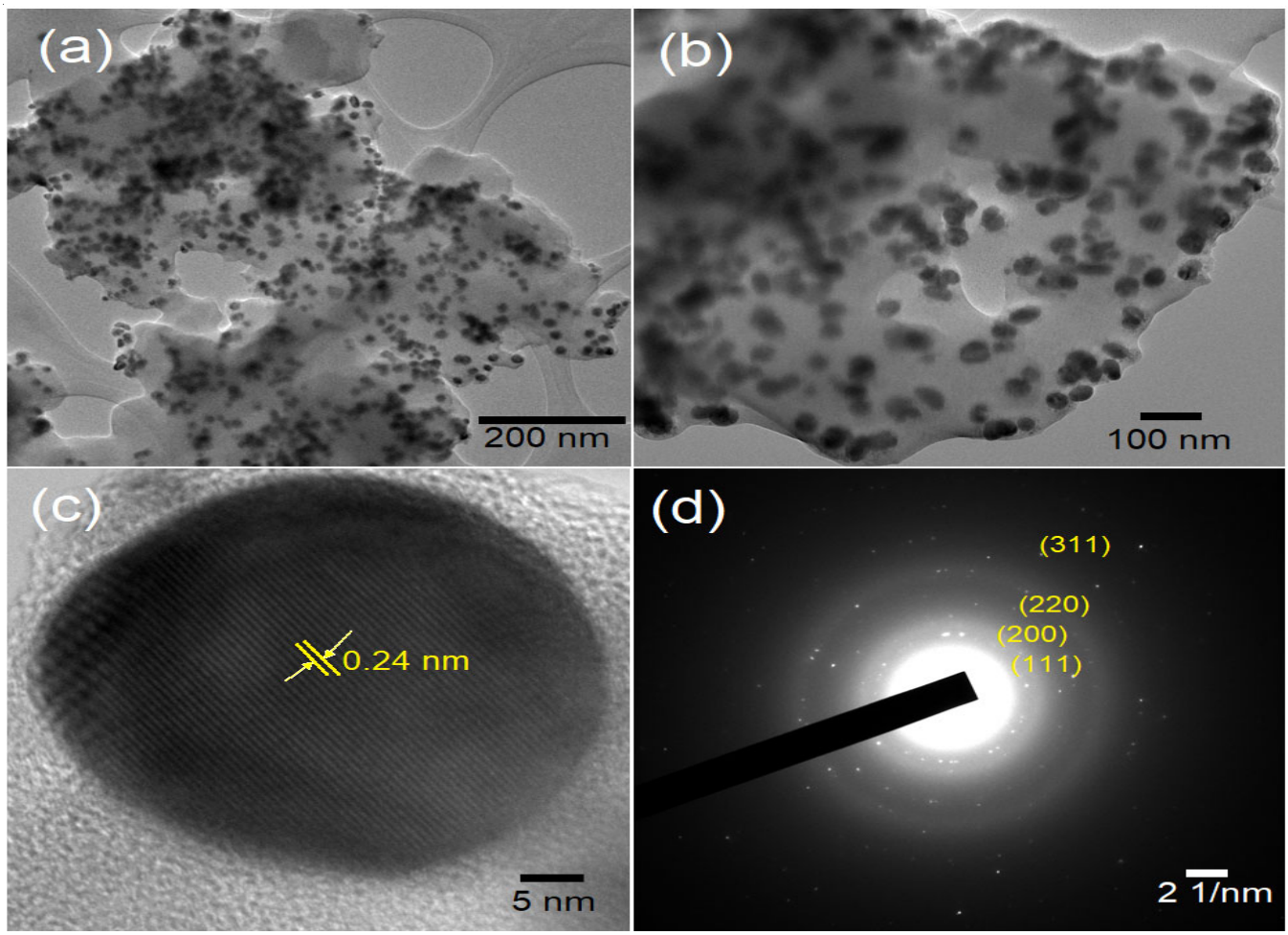

Fig. 7. TEM images of ZnO/Ag/MnO nanoparticles with (a) low magnification, (b) high magnification showing particles, (c) HRTEM showing lattice fringes and (d) electron diffraction image

under same pH, degradation studies were conducted at different light sources UV, visible and dark conditions. Investigations showed that the ZnO/Ag/MnO as catalyst is effective in visible light (Fig. 8). Hence further detailed studies were carried out under visible light.

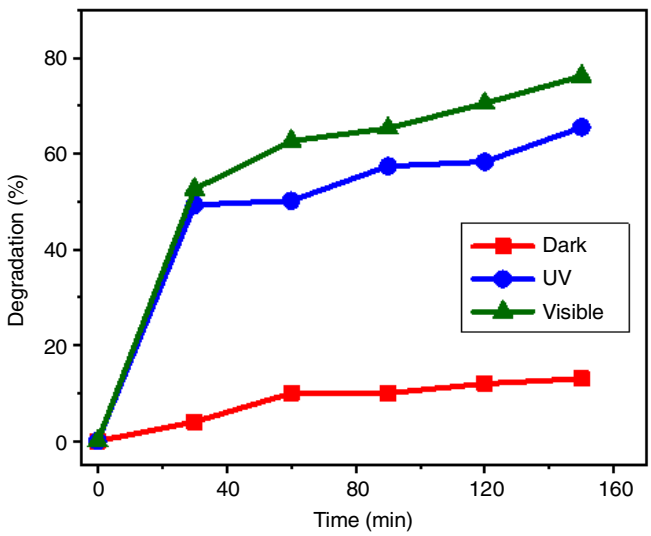

Fig. 8. Variation of light source on the degradation of methylene blue

Effect of dye concentration: The concentration of dye from 5 to 20 ppm was varied to study photocatalytic activities of ZnO/Ag/MnO nanoparticles. Photodegradation studies were carried out with a constant catalytic load of 40 mg at pH 7 and changing the concentration of dye from 5 to 20 ppm in sunlight (Fig. 9) to identify the suitable concentration of dye for effective degradation. It is noted that the reduction in the percentage of degradation with increased dye concentration from 10 to 80 ppm. Higher concentration of dye may reduce the dispersion of light radiation on the surface of catalyst which leads to a decrease in generation of hydroxyl radicals. This implies that UV light absorbed by methylene blue rather than photocatalyst.

Effect of catalyst concentration: By varying catalyst concentration in the range of 20 mg to 50 mg at the optimum 15 ppm of dye, the results indicated the percentage of dye degradation increased linearly with increased catalyst concentration. It was also noticed that there is a decrease in the degradation beyond 40 mg of a catalyst, which is due to agglomeration and sedimentation of the catalyst particles. This can be explained as an increase in catalyst concentration enhances the rate of adsorption of reactant molecules and hence the rate of reaction. Consequently, a considerable degradation of methylene blue was observed with a catalytic load of 40 mg (Fig. 10).

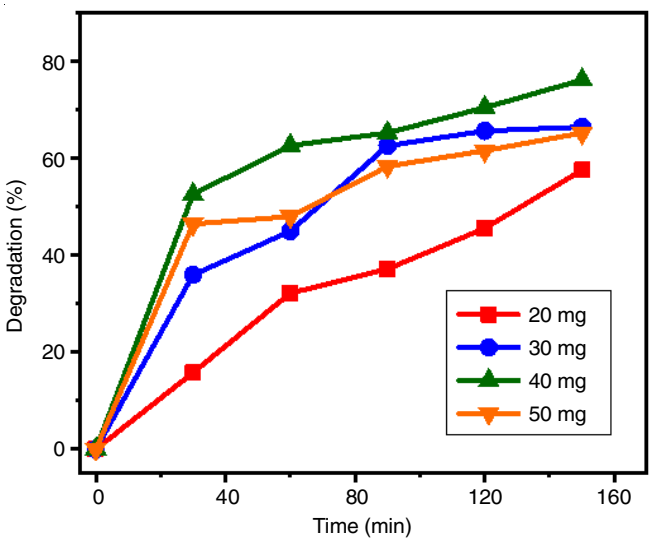

Fig. 10. Effect of catalytic load on the degradation of methylene blue

Effect of pH: Effect of pH on the photodegradation of methylene blue has been studied by varying pH by keeping dye and catalyst concentration optimum. Since the photodegradation is effective by the release of protons and maximum degradation (90.4%) was found at pH 10 (Fig. 11). A pH below 7, degradation decrease and nanoparticles have a surface charge that attracts a thin layer of ions of opposite charge to the surface. This can be explained by taking zero potential charge which is of 9 ± 0.3 for ZnO nanoparticles and above this level, the surface is negatively charged because of absorption of

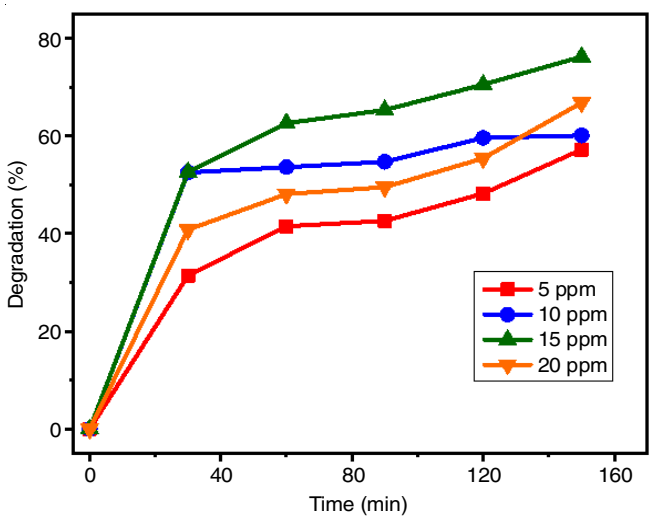

Fig. 9. Effect of dye concentration on the degradation of methylene blue

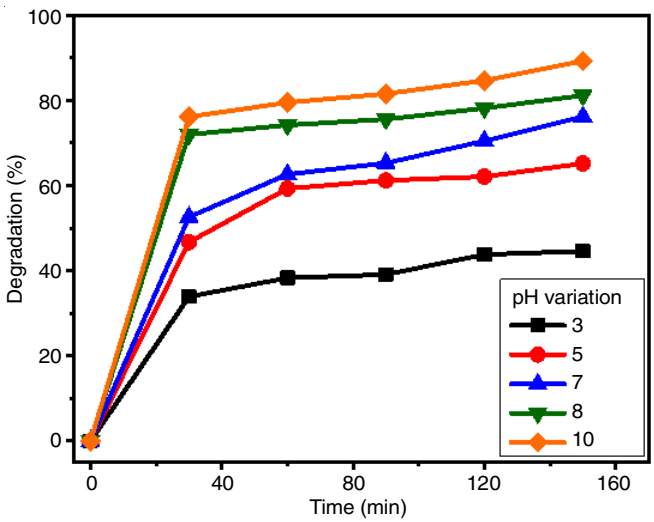

Fig. 11. Effect of pH on the degradation of methylene blue

hydroxyl ions. Due to the generation of more hydroxyl ions, the surface of the catalyst decreases for generation of hydroxyl radical. Hence, the minimal generation of hydroxyl radical′s degradation of dye decreases [26,27]. If the pH is in the range of 3 to 10, more absorption of dye on the surface of catalyst takes place.

Fig. 11 clearly indicates that pH of methylene blue solution had significant role on the photocatalytic activity of ZnO/Ag/MnO at above pH 10, methylene blue do not protonated due to the electrostatic repulsion between the surface charges on the adsorbent and the adsorbate prevents the absorption of methylene blue. Hence, the rate of degradation of methylene blue decreased at ≤ pH 10.

Mechanism: The degradation mechanism of the present study, wherein photogenerated electrons in the conduction band of semiconductors move to Ag nanoparticles and participated in the reduction reactions as shown in **Scheme-I**.

$$\text{Catalyst} + h\nu \longrightarrow \text{Catalyst}\,(h^{+}_{vb} + e^{-}_{cb})$$

$$OH^{-}_{ads} + h^{+}_{vb} \longrightarrow OH^{\bullet}_{ads}\,(\text{in alkaline condition})$$

$$MB + OH^{\bullet}_{ads} \longrightarrow \text{Degradtion products of MB}$$

Scheme-I

Conclusion

A ternary hybrid nanostructured ZnO-Ag-MnO was prepared hydrothermal method. The ternary composite showed a wide range of absorption by expanding absorption band both in UV and visible regions. Uniform distribution of ZnO, MnO and Ag was confirmed by FESEM and TEM morphologies. Heterostructure showed a significant photocatalytic degradation of methylene blue as well as enhanced photocatalytic activity under visible light.

ACKNOWLEDGEMENTS

The authors thank VGST (SMYSR-2016; GRD 506) Govt. of Karnataka, India for the financial support and Technical Research Centre-Microscopy lab at Jawaharlal Nehru Centre for Advanced Scientific Research (JNCASR), Bengaluru, India for providing the microscopy facilities.

CONFLICT OF INTEREST

The authors declare that there is no conflict of interests regarding the publication of this article.

REFERENCES

1. P. Pattnaik, G.S. Dangayach and A.K. Bhardwaj, *Rev. Environ. Health*, **33**, 163 (2018); https://doi.org/10.1515/reveh-2018-0013
2. R. Kant, *Nat. Sci.*, **4**, 22 (2012); https://doi.org/10.4236/ns.2012.41004
3. Puttaswamy, J.P. Shubha and R.V. Jagadeesh, *Transition Met. Chem*, **32**, 991 (2007); https://doi.org/10.1007/s11243-007-0271-x
4. Puttaswamy, K.N. Vinod and K.N.N. Gowda, *Dyes Pigments*, **78**, 131 (2008); https://doi.org/10.1016/j.dyepig.2007.11.002
5. D. Depan and R.D.K. Misra, *J. Biomed. Mater. Res. A*, **102**, 2934 (2014); https://doi.org/10.1002/jbm.a.34963
6. K. Manjunath, T.N. Ravishankar, D. Kumar, K.P. Priyanka, T. Varghese, H.R. Naika, H. Nagabhushana, S.C. Sharma, J. Dupont, T. Ramakrishnappa and G. Nagaraju, *Mater. Res. Bull.*, **57**, 325 (2014); https://doi.org/10.1016/j.materresbull.2014.06.010
7. N.S. Pavithra, K. Lingaraju, G.K. Raghu and G. Nagaraju, *Spectrochim. Acta A Mol. Biomol. Spectrosc.*, **185**, 11 (2017); https://doi.org/10.1016/j.saa.2017.05.032
8. Udayabhanu, G. Nagaraju, H. Nagabhushana, D. Suresh, C. Anupama, G.K. Raghu and S.C. Sharma, *Ceram. Int.*, **43**, 11656 (2017); https://doi.org/10.1016/j.ceramint.2017.05.351
9. D. Channei, B. Inceesungvorn, N. Wetchakun, S. Ukritnukun, A. Nattestad, J. Chen and S. Phanichphant, *Sci. Rep.*, **4**, 5757 (2014); https://doi.org/10.1038/srep05757
10. G. Nagaraju, K. Manjunath, T.N. Ravishankar, B.S. Ravikumar, H. Nagabhushan, G. Ebeling and J. Dupont, *J. Mater. Sci.*, **48**, 8420 (2013); https://doi.org/10.1007/s10853-013-7654-5
11. G. Nagaraju, J.P. Udayabhanu, J.P. Shubha, K. Manjunath and J. Dupont, *Int. J. Hydrogen Energy*, **43**, 4028 (2018); https://doi.org/10.1016/j.ijhydene.2017.10.092
12. K. Girija, S. Thirumalairajan, V.R. Mastelaro and D. Mangalaraj, *J. Mater. Chem. A Mater. Energy Sustain.*, **3**, 2617 (2015); https://doi.org/10.1039/C4TA05295A
13. S. Safa, R. Azimirad, S. Safalou Moghaddam and M. Rabbani, *Desal. Water Treat.*, **57**, 6723 (2016); https://doi.org/10.1080/19443994.2015.1012561
14. A. Phuruangrat, S. Siri, P. Wadbua, S. Thongtem and T. Thongtem, *J. Phys. Chem. Solids*, **126**, 170 (2019); https://doi.org/10.1016/j.jpcs.2018.11.007
15. E.E. Elemike, D.C. Onwudiwe, L. Wei, C. Lou and Z. Zhao, *J. Environ. Chem. Eng.*, **7**, 103190 (2019); https://doi.org/10.1016/j.jece.2019.103190
16. A.A. Essawy, *J. Cleaner Prod.*, **183**, 1011 (2018); https://doi.org/10.1016/j.jclepro.2018.02.214
17. T.K. Pathak, R.E. Kroon and H.C. Swart, *Vacuum*, **157**, 508 (2018); https://doi.org/10.1016/j.vacuum.2018.09.020
18. A. Khataee, R.D.C. Soltani, Y. Hanifehpour, M. Safarpour, H.G. Ranjbar and S.W. Joo, *Ind. Eng. Chem. Res.*, **57**, 1924 (2014); https://doi.org/10.1021/ie402743u
19. M.A. Hernandez-Carrillo, R. Torres-Ricardez, M.F. Garcia-Mendoza, E. Ramirez-Morales, L. Rojas-Blanco and L.L. Diaz-Flores, G.E. Sepúlveda-Palacios, F. Paraguay-Delgado and G. Pérez-Hernández, *Catal. Today*, **349**, 191 (2020); https://doi.org/10.1016/j.cattod.2018.04.060
20. J.R. Torres-Hernández, E. Ramírez-Morales, L. Rojas-Blanco, J. Pantoja-Enriquez, G. Oskam, F. Paraguay-Delgado, B. Escobar-Morales, M. Acosta-Alejandro, L.L. Díaz-Flores and G. Pérez-Hernández, *Mater. Sci. Semicond. Process.*, **37**, 87 (2015); https://doi.org/10.1016/j.mssp.2015.02.009
21. N. Morales-Flores, U. Pal and E. Sánchez Mora, *Appl. Catal. A Gen.*, **394**, 269 (2011); https://doi.org/10.1016/j.apcata.2011.01.011
22. J. Liqiang, S. Xiaojun, X. Baifu, W. Baiqi, C. Weimin and F. Honggang, *J. Solid State Chem.*, **177**, 3375 (2004); https://doi.org/10.1016/j.jssc.2004.05.064
23. N. Karimizadeh, M. Babamoradi, R. Azimirad and M. Khajeh, *J. Electron. Mater.*, **47**, 5452 (2018); https://doi.org/10.1007/s11664-018-6427-y
24. P. Bharathi, S. Harish, J. Archana, M. Navaneethan, S. Ponnusamy, C. Muthamizhchelvan, M. Shimomura and Y. Hayakawa, *Appl. Surf. Sci.*, **484**, 884 (2019); https://doi.org/10.1016/j.apsusc.2019.03.131
25. J. Li, F. Zhao, L. Zhang, M. Zhang, H. Jiang, S. Li and J. Li, *RSC Adv.*, **83**, 67610 (2015); https://doi.org/10.1039/C5RA08903D
26. S. Chu, H. Li, Y. Wang, Q. Ma, H. Li, Q. Zhang and P. Yang, *Mater. Lett.*, **252**, 219 (2019); https://doi.org/10.1016/j.matlet.2019.05.145

27. Y. Liu, G. Li, R. Mi, C. Deng and P. Gao, *Sens. Actuators B Chem.*, **191**, 537 (2014); https://doi.org/10.1016/j.snb.2013.10.068
28. B.L. Martínez-Vargas, M. Cruz-Ramírez, J.A. Díaz-Real, J.L. Rodríguez-López, F.J. Bacame-Valenzuela, R. Ortega-Borges, Y. Reyes-Vidal and L. Ortiz- Frade, *J. Photochem. Photobiol. Chem.*, **369**, 85 (2019); https://doi.org/10.1016/j.jphotochem.2018.10.010
29. P. Latha, K. Prakash and S. Karuthapandian, *Adv. Powder Technol.*, **28**, 2903 (2017); https://doi.org/10.1016/j.apt.2017.08.017
30. S.B. Atla, W.-R. Lin, T.-C. Chien, M.-J. Tseng, J.-C. Shu, C.-C. Chen and C.-Y. Chen, *Mater. Chem. Phys.*, **216**, 380 (2018); https://doi.org/10.1016/j.matchemphys.2018.06.020
31. E. Acayanka, D.S. kuete, G.Y. Kamgang, S. Nzali, S. Laminsi and P.T. Ndifon, *Plasma Chem. Plasma Process.*, **36**, 799 (2016); https://doi.org/10.1007/s11090-016-9699-0
32. L. Wang, S. Liu, Z. Wang, Y. Zhou, Y. Qin and Z.L. Wang, *ACS Nano*, **10**, 2636 (2016); https://doi.org/10.1021/acsnano.5b07678
33. K. Manjunath, V.S. Souza, T. Ramakrishnappa, G. Nagaraju, J.D. Scholten and J. Dupont, *J. Mater. Res. Exp.*, **3**, 115904 (2016); https://doi.org/10.1088/2053-1591/3/11/115904
34. Z. Zhang, Y. Ma, X. Bu, Q. Wu, Z. Hang, Z. Dong and X. Wu, *Sci. Rep.*, **8**, 10532 (2018); https://doi.org/10.1038/s41598-018-28832-w
35. S.R. Lingampalli, U.K. Gautam and C.N.R. Rao, *Energy Environ. Sci.*, **6**, 3589 (2013); https://doi.org/10.1039/c3ee42623h
36. H. Tedla, I. Díaz, T. Kebede and A.M. Taddesse, *J. Environ. Chem. Eng.*, **3**, 1586 (2015); https://doi.org/10.1016/j.jece.2015.05.012
37. V. Hoseinpour and N. Ghaemi, *Mater. Res. Express*, **5**, 085012 (2018); https://doi.org/10.1088/2053-1591/aad2c6
38. J. Nagaraju and S. Pranesh, *Curr. Nanomater.*, **5**, 36 (2020); https://doi.org/10.2174/2405461504666191202105734